Microgrids energy management using robust convex programming

Microgrids Energy Management Using Robust Convex Programming

Juan S. Giraldo, Jhon A. Castrillon, Juan Camilo López, Marcos J. Rider, *Senior Member, IEEE* and Carlos A. Castro, *Senior Member, IEEE*

***Abstract*—This paper presents an energy management system (EMS) for single-phase or balanced three-phase microgrids via robust convex optimization. Along a finite planning horizon, the solution provided by the proposed microgrids EMS remains feasible under adverse conditions of random demands and renewable energy resources. The proposed model is represented as a convex mixed-integer second-order cone programming model. Two operation modes are considered: grid-connected and isolated modes. In grid-connected mode, the proposed EMS minimizes the costs of energy imports, dispatches of distributed generation (DG) units, and the operation of the energy storage systems. In isolated mode, the proposed EMS minimizes the unsupplied demand, considering consumer priorities. Global robustness of the proposed mathematical model is adjusted using a single parameter ζ. The robustness of the solutions provided by the robust EMS is assessed using the Monte Carlo simulation method. In this case, DG units are set to operate in frequency and voltage droop control to support network fluctuations. Simulations are deployed using a microgrid with 136-nodes and several distributed energy resources. Results showed that the proposed model is suitable for the short-term microgrids energy management system. The robustness of the final solution was directly proportional to the operational costs, and it can be effectively controlled by the proposed parameter ζ for both operation modes. When compared to stochastic approaches, the proposed formulation showed to be more flexible and less time-consuming.**

***Index Terms*—Energy management system, microgrids, mixed-integer second-order cone programming, robust convex optimization.**

NOMENCLATURE

Sets

Ω_b	Set of nodes.
Ω_{DG}	Set of nodes with distributed generation (DG) units.
Ω_{ESS}	Set of nodes with energy storage systems (ESS).
Ω_l	Set of lines.
Ω_{PV}	Set of nodes with photo-voltaic (PV) units.
Ω_{S}	Point of common coupling (PCC).
Ω_{T}	Set of time periods.
Ω_{WT}	Set of nodes with wind turbine (WT) units.

Parameters

$c_b^{\mathrm{ESS,ch}}$	Charging cost of the ESS at node b [\$/kWh].
$c_b^{\mathrm{ESS,dc}}$	Discharging cost of the ESS at node b [\$/kWh].
c_g^{DG}	Unitary cost of the DG unit at node g [\$/kWh].
c_i^{ls}	Cost of load shedding at node i [\$/kWh].
c_t^{S}	Cost of energy imports at period t [\$/kWh].
EC_b	Energy capacity of the ESS at node b [kWh].
$\underline{\mathrm{F}}_g$	Minimum fuel of the DG unit at node g [m^3].
FC_g	Fuel capacity of the DG unit at node g [m^3].
H_g	Calorific value of the DG unit at node g [kWh/m^3].
$\overline{I}_{ij}$	Maximum current magnitude for line ij [A].
$P_{i,t}^{\mathrm{D}}$	Robust active demand at node i, period t [kW].
pf_{g}	Power factor limit of the DG unit at node g.
$P_{g,t}^{\mathrm{sp}}$	Active power set-point of the DG unit at node g, period t [kW].
$P_{b,t}^{\mathrm{sp}}$	Active power set-point of the ESS unit at node b, period t [kW].
$P_{p,t}^{\mathrm{PV}}$	Robust PV production at node p, period t [kW].
$P_{\omega,t}^{\mathrm{WT}}$	Robust WT production at node ω, period t [kW].
$Q_{i,t}^{\mathrm{D}}$	Robust reactive demand at node i, period t [kvar].
$Q_{g,t}^{\mathrm{sp}}$	Reactive power set-point of the DG unit at node g, period t [kvar].
$\mathrm{R}_g^{\mathrm{up}}$	Ramp-up limit of the DG unit at node g [kW/h].
$\mathrm{R}_g^{\mathrm{dw}}$	Ramp-down limit of the DG unit at node g [kW/h].
R_{ij}	Resistance of line ij [mΩ].
$\overline{\mathrm{S}}_g^{\mathrm{DG}}$	Maximum capacity for DG unit at node g [kVA].
$\overline{S}_i^{\mathrm{S}}$	Substation capacity at node i [kVA].
$\overline{\mathrm{SOC}}_b$	Maximum SOC of the ESS at node b [%].
$\underline{\mathrm{SOC}}_b$	Minimum SOC of the ESS at node b [%].
SOC_b^{τ}	Minimum SOC at period τ of the ESS at node b [%].
$\overline{V}$	Maximum voltage magnitude [kV].
$\underline{V}$	Minimum voltage magnitude [kV].
X_{ij}	Reactance of line ij [mΩ].
$\alpha_{p,t}$	Shape of PV production at node p, period t.
$\beta_{p,t}$	Rate of PV production at node p, period t.
Δ_t	Time period length at period t [h].
$\overline{\Delta f}$	Maximum frequency variation [Hz].
$\underline{\Delta f}$	Minimum frequency variation [Hz].
ζ	Robustness adjustment parameter.
η_b^{dc}	Discharging efficiency of the ESS at node b.
η_b^{ch}	Charging efficiency of the ESS at node b.
η_g^{f}	Fuel efficiency of DG unit at node g.
θ_g^{f}	Frequency droop of the DG unit at node g [kW/Hz].

This work was financially supported by the Brazilian institutions CNPq, CAPES, and FAPESP research grant $2015/12564-1$. All authors are with the Department of Systems and Energy, University of Campinas, Campinas, SP, Brazil. e-mail: {jnse; jacastri; jclopeza; mjrider}@dsee.fee.unicamp.br, ccastro@ieee.org.

θ_g^{v} Voltage droop of the DG unit at node g [V/Hz].
$\kappa_{\omega,t}$ Shape for WT unit at node ω, period t.
$\lambda_{\omega,t}$ Scale for WT unit at node ω, period t.
$\mu_{i,t}^{\mathrm{P}}$ Mean active demand at node i, period t [kW].
$\mu_{i,t}^{\mathrm{Q}}$ Mean reactive demand at node i, period t [kvar].
ξ_b Self-discharging rate of the ESS at node b [%].
$\rho_{i,t}$ Demand correlation at node i, period t.
$\sigma_{i,t}^{\mathrm{P}}$ Std. dev. of active demand at node i, period t [kW].
$\sigma_{i,t}^{\mathrm{Q}}$ Std. dev. of reactive demand at node i, period t [kvar].
Υ Robustness adjustment parameter for different probability distribution functions.

Variables

$F_{g,t}$ Remaining fuel of DG unit at node g, period t [%].
I_{ij}^{sqr} Squared current magnitude at line ij [A^2].
$P_{ij,t}$ Active power flow at line ij, period t [kW].
$P_{b,t}^{\mathrm{ESS,ch}}$ Charging power of the ESS at node b, period t [kW].
$P_{b,t}^{\mathrm{ESS,dc}}$ Discharging power of ESS at node b, period t [kW].
$P_{g,t}^{\mathrm{DG}}$ Active production of the DG at node g, period t [kW].
$P_{i,t}^{\mathrm{S}}$ Active power injection at substation i, period t [kW].
$Q_{ij,t}$ Reactive power flow at line ij, period t [kvar].
$Q_{g,t}^{\mathrm{DG}}$ Reactive production of DG at node g, period t [kvar].
$Q_{i,t}^{\mathrm{S}}$ Reactive power injection at substation i, period t [kvar].
$\mathrm{SOC}_{b,t}$ SOC of the ESS at node b, period t [%].
$V_{i,t}^{\mathrm{sqr}}$ Squared voltage magnitude at node i, period t [kV^2].
Δf_t Frequency variation at period t [Hz].
$\Lambda_{b,t}$ Binary variable associated to the charging operation of the ESS at node b, period t.
$\Pi_{g,t}$ Binary variable associated to the unit commitment of the DG unit at node g, period t.
$\Phi_{b,t}$ Binary variable associated to the discharging operation of the ESS at node b, period t.
$\Psi_{i,t}$ Binary variable associated to the load shedding at node i, period t.

I. Introduction

MICROGRIDS have gained a lot of attention because they have not only a positive impact on the integration of renewable energy sources (RES) but also they could be used to improve the overall performance of the electrical grid [1]. A microgrid is defined as a cluster of distributed energy resources, storage devices and loads, connected to a main grid through a controllable switch, that provides reliable and secure electrical power to a local community [2]. A major advantage of microgrids is their flexibility to operate in grid-connected or islanded mode. In this context, a microgrid energy management system (EMS) is a set of hardware/software components used to efficiently operate the energy resources of the microgrid by typically, but not exclusively, scheduling the commitment of dispatchable distributed generation (DG) units, energy storage systems (ESS), energy imports, and controllable loads, to achieve selected objectives. Clearly, random nature of RES, such as wind turbines (WTs) and photovoltaics (PV) units, as well as conventional demands, should be a major concern when optimizing the operation of the microgrid in a given planning horizon [3].

Up to now, several deterministic approaches for microgrids EMS have been already proposed. In [4], a centralized EMS using forecasted injections was presented. Then, authors in [5] proposed a similar heuristic EMS, based on an active power flow. A mixed-integer linear programming model for the modeling and experimental verification of an EMS was proposed in [6], and finally, a mixed-integer second-order cone programming (MISOCP) model for isolated microgrids was proposed in [7]; however, the uncertainty of the forecasted parameters was not considered. Uncertainties in some parameters have also been studied, as in [8] and [9], where loads and PV production were included as stochastic variables within a scenario-based approach. Authors in [10] proposed a multi-objective stochastic programming model, considering RES and demand response, based on a simplified active power flow, while in [11] authors proposed a stochastic framework for the day-ahead scheduling of ESS in microgrids using the genetic algorithm, and in [12] an approximated dynamic programming algorithm was used for the stochastic economic dispatch of microgrids.

Robust optimization is another suitable tool for considering volatility on random variables within the optimization process. Compared to stochastic programming, robust optimization problems are less challenging to be solved because they do not require to operate over multiple probable scenarios. In this case, robust approaches create deterministic equivalents of an essentially stochastic optimization problem, rather than a discretized representation of the probability density functions (PDFs) of the random phenomena [13]. As indicated in [14] and [15], robust models generate optimized solutions that remain feasible, even if numerous exogenous variables are randomly changing at the same time. Since deterministic convex optimization models are tractable, so are their robust counterparts [13], making it possible to find an optimal solution using commercial solvers.

Consequently, authors in [16] proposed a linear robust EMS with high penetration of RES, considering the worst-case transaction cost. Similarly, authors in [17] proposed a robust EMS using a fuzzy predictive control model for wind production. In [3], a robust optimization model was also used to incorporate RES and load variability. A distributed robust EMS for smart grids is proposed in [18] using a non-linear approach. Authors in [19] proposed a chance-constrained programming model for the EMS of grid-connected microgrids, while a robust two-stage model was proposed in [20] using a mixed-integer linear programming formulation. A robust model for islanding-aware microgrids EMS with RES and co-generation was proposed in [21], while in [22] authors proposed a chance-constrained EMS for islanded microgrids. However, none of the aforementioned works considered the presence of reactive power flow, which is essential for the EMS in practical systems. Especially, if the isolated operation mode is considered. On the other hand, authors in [23] proposed a chance-constrained AC optimal power flow for distribution systems

considering RES, while authors in [24] proposed a non-linear, non-convex, robust framework for active and reactive power management in distribution networks using electric vehicles. However, the isolated mode is neither discussed in [23] nor in [24]. Finally, the use of a robust-convex chance-constrained formulation was proposed in [25]. However, the convexity of the problem in [25] is limited by the characteristics of the random variables, which are required to be approximately Gaussian distributed, and the relationships between the state and control variables are required to be linear.

In this context, this paper proposes a robust convex optimization model for the EMS of single-phase or balanced three-phase microgrids using a MISOCP model. The proposed model considers an AC power flow, grid-connected/isolated operation modes, guarantees global optimality, and global robustness is attained by a single setting parameter. To the best of our knowledge, no MISOCP model with those characteristics has been proposed to deploy an EMS of microgrids [26]. The proposed model integrates dispatchable DG units, ESS, load shedding, and stochasticity over conventional demands and non-dispatchable PV and WT units. Since the proposed formulation assumes that a previous short-term forecast has been made for RES as in [27], and for loads as in [28], it is considered as a short-term planning problem [29]. Global robustness is adjusted using a single parameter ζ, and the convexity of the formulation does not depend on the characteristics of the random variables' PDFs. Furthermore, an intuitive procedure to calculate suitable values of ζ for all random variables is presented in this paper. A major advantage of using a MISOCP model is it convexity. As shown in [30] and [31], under most circumstances, the optimal solution of the MISOCP model is equivalent to the optimal solution of the original non-linear non-convex model.

Solutions obtained with the proposed robust model will be compared to a stochastic approach using the sample average approximation (SAA) method [32], in terms of computational burden and the robustness of the final solution. Global robustness of final solutions will be assessed by submitting the decisions provided by the EMS to several random scenarios using Monte Carlo simulation (MCS). In this case, the EMS provides the optimal set-points, whereas the frequency and voltage droop control of the dispatchable DG units supports the network. The proposed EMS has been tested on a 136-nodes system, adapted to consider multiple dispatchable DG units, ESS and RES, resembling a campus area or an industrial microgrid.

II. Characterization of Robust Parameters

According to [14] and [33], the term *robust optimization* is used to denote a set of optimization techniques whose solutions remain feasible under uncertainty of exogenous parameters. Robust optimization aims at finding the solution that minimizes the objective function while remains feasible for most probable outcomes of random phenomena. As mentioned in [14], robust optimization models can cope with uncertainty embedded into inequality constraints and in the objective function. However, equality constraints are usually not addressed by most robust design methods. When dealing with robust optimization models, equality constraints can be classified into two categories [34]: Type I, which are constraints that must be strictly satisfied, regardless of the realizations of the random variables, and Type II constraints, which cannot be strictly satisfied because of uncertainty [35]. Since equality constraints in this paper are all associated to physical laws, e.g., Kirchhoff's circuit laws, energy balance equations, etc., then all equality constraints fit into the Type I category and no further analysis is required.

A. Robust Convex Optimization

Consider the linear optimization problem in (1)–(3).

$$\min \quad \textstyle\sum_j c_j x_j \tag{1}$$

subject to:

$$\textstyle\sum_j a_{ij} x_j = b_i \quad \forall i \tag{2}$$

$$l_j \le x_j \le u_j \quad \forall j \tag{3}$$

where x_j represents the j-th variable, bounded by lower and upper limits l_j and u_j. Weights at the objective function are given by c_j. Coefficients a_{ij} for each constraint i and variable j are considered as known parameters, whereas the independent terms b_i in (2) are exogenous random variables.

Considering that b_i can be characterized by a known PDF whose cumulative distribution function (CDF) is given by CDF_{b_i}, the probability of b_i being lower or equal than its expected value is $\tilde{\text{P}}_{b_i} = \Pr\left(b_i \le \mu_i^b\right) = \text{CDF}_{b_i}\left(\mu_i^b\right)$. Then, a robust equivalent of constraint (2) can be expressed as in (4)–(5), where B_i is a robust equivalent of b_i.

$$\textstyle\sum_j a_{ij} x_j = B_i = \text{CDF}_{b_i}^{-1}\left(\tilde{\text{P}}_{b_i} \pm \zeta\right) \quad \forall i \tag{4}$$

$$\zeta \in \mathbb{R} : \left\{0 < \tilde{\text{P}}_{b_i} \pm \zeta < 1\right\} \quad \forall i \tag{5}$$

Note that global robustness of the optimization model can be adjusted by the single parameter ζ in (4). The sign in (4) is chosen according to the nature of the random variable b_i. Condition (5) guarantees that only probable values of b_i will be used as robust equivalents.

Figure 1 illustrates the meaning of the robustness adjustment parameter ζ, in which probabilities $\tilde{\text{P}}_{b_i}^p$ and $\tilde{\text{P}}_{b_i}^o$, produce the robust equivalents B_i^p and B_i^o, respectively. For the sake of clarity, assume that b_1 represents a random variable in which a more robust scenario requires its value to be greater than the expected value, i.e., loads. On the other hand, b_2 represents another random variable in which its robust equivalent must be lower than its expected value to obtain a robust scenario, i.e., renewable generation resources.

Notice that robust equivalents B_i^p and B_i^o depend on the nature of each random variable b_1 and b_2, which is related to the sign in (4), along with the value set for ζ. This leads to three possible situations:

a) $\zeta > 0 \rightarrow B_1^p > \mu_1$, and $B_2^p < \mu_2$.
b) $\zeta < 0 \rightarrow B_1^o < \mu_1$, and $B_2^o > \mu_2$.
c) $\zeta = 0 \rightarrow B_i^p = \mu_i = B_i^o, \forall\, i = 1, 2$.

Situation a) produces a *pessimist* scenario, in which load equivalents are greater than the average and generations from RES are lower than the average, leading to a more robust

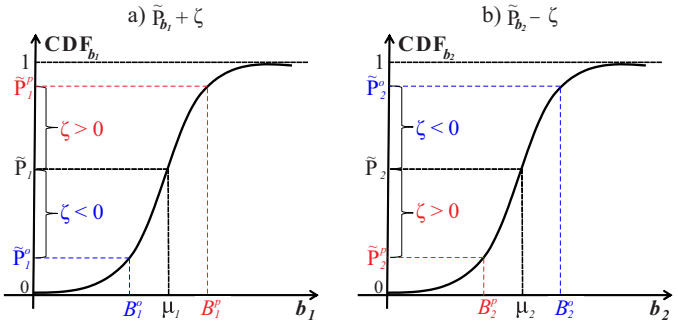

Fig. 1. Meaning of the robustness adjustment parameter ζ for loads (a) and RES (b).

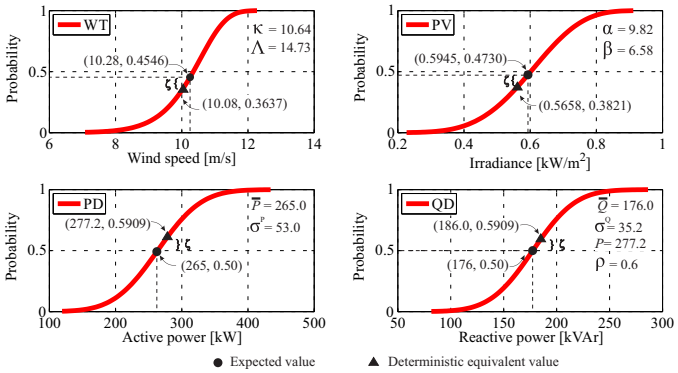

Fig. 2. Illustrative example for choosing ζ, based on $\Upsilon = 0.6$ and different types of CDFs.

solution. Situation b) produces an *optimist* scenario, in which load equivalents are lower than their average and generation equivalents are greater than their average, leading to a less robust solution. Finally, situation c) produces the deterministic average scenario, where all random variables are fixed to their respective expected outcomes.

B. Robust Equivalents for RES

Solar irradiation for a PV unit at bus p and period t is assumed to follow a beta distribution function described by its shape and rate parameters as in (6). Similarly, wind velocities of a WT unit at bus w and period t is described by its shape and scale parameters following a Weibull PDF, as in (7). Considering that a reduction in solar irradiance and in wind velocity reflects a proportional lower power production, robust equivalents are obtained assuming that RES behave as in Fig. 1b. Thus, they are obtained by fixing the sign in (4) to be negative, as shown in (8) and (9).

$$p_{p,t}^{\mathrm{PV}} \sim \mathrm{Beta}\left(\alpha_{p,t}, \beta_{p,t}\right) \qquad \forall p \in \Omega_{\mathrm{PV}},\ t \in \Omega_{\mathrm{T}} \quad (6)$$

$$p_{p,t}^{\mathrm{WT}} \sim \mathrm{Weibull}\left(\kappa_{\omega,t}, \lambda_{\omega,t}\right) \qquad \forall \omega \in \Omega_{\mathrm{WT}},\ t \in \Omega_{\mathrm{T}} \quad (7)$$

$$P_{p,t}^{\mathrm{PV}} = \mathrm{CDF}_{p,t}^{-1}\left(\tilde{\mathrm{P}}_{p,t}^{\mathrm{PV}} - \zeta\right) \qquad \forall p \in \Omega_{\mathrm{PV}},\ t \in \Omega_{\mathrm{T}} \quad (8)$$

$$P_{\omega,t}^{\mathrm{WT}} = \mathrm{CDF}_{\omega,t}^{-1}\left(\tilde{\mathrm{P}}_{\omega,t}^{\mathrm{WT}} - \zeta\right) \qquad \forall \omega \in \Omega_{\mathrm{WT}},\ t \in \Omega_{\mathrm{T}} \quad (9)$$

It should be stated that RES are operating at unity power factor in this formulation. However, if required, reactive components of RES can be easily included as power injections.

C. Robust Equivalents for Demands

Conventional demands are considered to follow a bivariate normal PDF to account for the correlation between active and reactive power components as in (10), where $\mathbf{a} = \left[\mu_{i,t}^{\mathrm{P}}; \sigma_{i,t}^{\mathrm{P}}; \mu_{i,t}^{\mathrm{Q}}; \sigma_{i,t}^{\mathrm{Q}}\right]$. Robust equivalents associated with conventional demands at node i and period t would consist of having higher consumption. They are obtained assuming that loads behave as in Fig. 1a. Thus, the sign in (4) is set to be positive for active and reactive power as shown in (11), in which values of $Q_{i,t}^{\mathrm{D}}$ and $P_{i,t}^{\mathrm{D}}$ are correlated.

$$p_{i,t}^{\mathrm{D}}, q_{i,t}^{\mathrm{D}} \sim \mathcal{N}_{\mathrm{bivariate}}\left(\mathbf{a}, \rho_{i,t}\right) \qquad \forall i \in \Omega_b,\ t \in \Omega_{\mathrm{T}} \quad (10)$$

$$P_{i,t}^{\mathrm{D}}, Q_{i,t}^{\mathrm{D}} = \mathrm{CDF}_{i,t}^{-1}\left(\tilde{\mathrm{P}}_{i,t}^{p} + \zeta, \tilde{\mathrm{P}}_{i,t}^{q} + \zeta\right) \quad \forall i \in \Omega_b, t \in \Omega_{\mathrm{T}} \quad (11)$$

D. Robustness Adjustment Parameter ζ

Suitable values for ζ are often challenging to obtain if all variables do not follow identical PDFs. Thus, an intuitive procedure for setting ζ is shown in (12) for any stochastic variable with known probability distribution. As established in Section II-A, the sign in (4) is different for loads and RESs, thus, this condition must be reflected in the portion of the CDF selected by Υ. The robustness adjustment parameter ζ is selected as in (12) guaranteeing that the asymptotic limits of each CDF are respected. Eq. (12) presents a linear relationship for an arbitrary value $0 < \Upsilon < 1$, where $A = \min\{\underline{P}, 1 - \overline{P}\}$ with $\overline{P} = \max\{\tilde{\mathrm{P}}_{i,t}^{p}, \tilde{\mathrm{P}}_{i,t}^{q}, \tilde{\mathrm{P}}_{p,t}^{\mathrm{PV}}, \tilde{\mathrm{P}}_{\omega,t}^{\mathrm{WT}}\}$, and $\underline{P} = \min\{\tilde{\mathrm{P}}_{i,t}^{p}, \tilde{\mathrm{P}}_{i,t}^{q}, \tilde{\mathrm{P}}_{p,t}^{\mathrm{PV}}, \tilde{\mathrm{P}}_{\omega,t}^{\mathrm{WT}}\}$.

$$\zeta = A\left(2\Upsilon - 1\right) \quad (12)$$

Note that $\Upsilon \approx 0$ relates an extremely *optimist* scenario, while $\Upsilon \approx 1$ represents a *pessimist* one. As an example, assume a node with a PV unit, a WT, and conventional demands represented as random variables. Their respective CDFs, expected values, and shape parameters are shown in Fig. 2. Let $\tilde{\mathrm{P}}_{i,t}^{p} = 0.5$, $\tilde{\mathrm{P}}_{i,t}^{q} = 0.5$, $\tilde{\mathrm{P}}_{p,t}^{\mathrm{PV}} = 0.47$, and $\tilde{\mathrm{P}}_{p,t}^{\mathrm{WT}} = 0.45$. In this case $\overline{P} = 0.5$, and $\underline{P} = 0.45$, thus, $A = \underline{P}$. Consequently, for an arbitrary $\Upsilon = 0.60$ it can be seen that $\zeta = 0.09$ is obtained. The deterministic equivalents for all random variables using (8), (9), and (11) are shown in Fig. 2.

III. Proposed Robust Micogrids EMS

Once the robust equivalents of RES and demands have been characterized using parameter ζ, this section presents the objective function and constraints of the proposed robust EMS.

A. Objective Function

The objective function is shown by (13), relating the cost of the imported energy from the utility grid in the first term. The second term represents the cost of the energy produced by dispatchable DG units. The third embodies the cost of injected (discharging) or absorbed (charging) energy by the ESS, the fourth considers the cost of deploying load shedding on the nodes.

$$\min \sum_{t\in\Omega_T}\Delta_t\Bigg\{\sum_{i\in\Omega_b} c_t^{\mathrm{S}} P_{t,i}^{\mathrm{S}} + \sum_{g\in\Omega_{\mathrm{DG}}} c_g^{\mathrm{DG}} P_{g,t}^{\mathrm{DG}} + \sum_{b\in\Omega_{\mathrm{ESS}}}\left(c_b^{\mathrm{ESS,dc}} P_{b,t}^{\mathrm{ESS,dc}} - c_b^{\mathrm{ESS,ch}} P_{b,t}^{\mathrm{ESS,ch}}\right) + \sum_{i\in\Omega_b} c_i^{\mathrm{ls}}\left(\Psi_{i,t} P_{i,t}^{\mathrm{D}}\right)\Bigg\} \tag{13}$$

B. Microgrid's Steady-state Operation

Active and reactive power flows are represented by (14) and (15). Since current and voltage magnitudes appear naturally as squared, non-negative, continuous variables in the steady-state operation of AC electrical distribution networks, it is convenient to perform the change in variables $V_{i,t}^{\mathrm{sqr}} \equiv V_{i,t}^2$ and $I_{ij,t}^{\mathrm{sqr}} \equiv I_{ij,t}^2$ as in [31], to obtain a convex second-order cone equivalent.

$$\sum_{ki\in\Omega_l} P_{ki,t} - \sum_{ij\in\Omega_l}\left(P_{ij,t} + R_{ij} I_{ij,t}^{\mathrm{sqr}}\right) + P_{i,t}^{\mathrm{S}} + \sum_{g\in\Omega_{\mathrm{DG}}|_{g=i}} P_{g,t}^{\mathrm{DG}} + \sum_{b\in\Omega_{\mathrm{ESS}}|_{b=i}}\left(P_{b,t}^{\mathrm{ESS,dc}} + P_{b,t}^{\mathrm{ESS,ch}}\right) = \left(1-\Psi_{i,t}\right) P_{i,t}^{\mathrm{D}} - \sum_{p\in\Omega_{\mathrm{PV}}|_{p=i}} P_{p,t}^{\mathrm{PV}} - \sum_{\omega\in\Omega_{\mathrm{WT}}|_{\omega=i}} P_{\omega,t}^{\mathrm{WT}} \quad \forall i\in\Omega_b, t\in\Omega_{\mathrm{T}} \tag{14}$$

$$\sum_{ki\in\Omega_l} Q_{ki,t} - \sum_{ij\in\Omega_l}\left(Q_{ij,t} + X_{ij} I_{ij,t}^{\mathrm{sqr}}\right) + Q_{i,t}^{\mathrm{S}} + \sum_{g\in\Omega_{\mathrm{DG}}|_{g=i}} Q_{g,t}^{\mathrm{DG}} = \left(1-\Psi_{i,t}\right) Q_{i,t}^{\mathrm{D}} \quad \forall i\in\Omega_b, t\in\Omega_{\mathrm{T}} \tag{15}$$

$$P_{i,t}^{\mathrm{S}} = Q_{i,t}^{\mathrm{S}} = 0.0 \quad \forall i\in\Omega_b, t\in\Omega_{\mathrm{T}} : i\notin\Omega_{\mathrm{S}} \tag{16}$$

$$\Psi_{i,t}\in\{0,1\} \quad \forall i\in\Omega_b, t\in\Omega_{\mathrm{T}} \tag{17}$$

Robust parameters are displayed after the equal sign in (14) for active power components, as well as in (15) for reactive power components, while (16) guarantees that only nodes with active sources are able to inject power. The binary variable associated to load shedding is defined in (17). Notice that RES are operating at unity power factor. However, if required, reactive components of RES can be easily included in the balance equation (15). Voltage magnitude drop between nodes i and j is represented by (18). Minimum and maximum nodal voltage magnitudes are limited by (19), and current magnitudes are calculated with (20) through a conic inequality, and limited by (21). A set of sufficient conditions for (20) to be activated is provided in [30]. At last, a quadratic convex constraint is presented in (22) for limiting the substation capacities.

$$V_{i,t}^{\mathrm{sqr}} - 2\left(R_{ij}P_{ij,t} + X_{ij}Q_{ij,t}\right) - \left(R_{ij}^2 + X_{ij}^2\right) I_{ij,t}^{\mathrm{sqr}} = V_{j,t}^{\mathrm{sqr}} \quad \forall ij\in\Omega_l, t\in\Omega_{\mathrm{T}} \tag{18}$$

$$\underline{V}^2 \le V_{i,t}^{\mathrm{sqr}} \le \overline{V}^2 \quad \forall i\in\Omega_b, t\in\Omega_{\mathrm{T}} \tag{19}$$

$$V_{j,t}^{\mathrm{sqr}} I_{ij,t}^{\mathrm{sqr}} \ge P_{ij,t}^2 + Q_{ij,t}^2 \quad \forall ij\in\Omega_l, t\in\Omega_{\mathrm{T}} \tag{20}$$

$$0 \le I_{ij,t}^{\mathrm{sqr}} \le \overline{I_{ij}}^2 \quad \forall ij\in\Omega_l, t\in\Omega_{\mathrm{T}} \tag{21}$$

$$\left(P_{i,t}^{\mathrm{S}}\right)^2 + \left(Q_{i,t}^{\mathrm{S}}\right)^2 \le \left(\overline{S}_i^{\mathrm{S}}\right)^2 \quad \forall i\in\Omega_b, t\in\Omega_{\mathrm{T}} \tag{22}$$

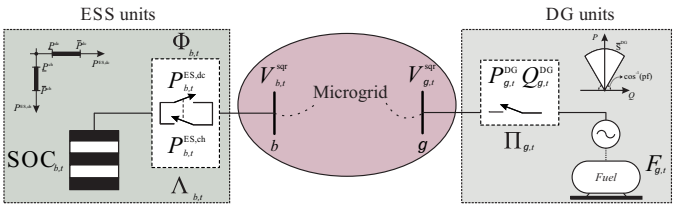

Fig. 3. Representation of the models used for ESS and DG units.

Dispatchable DG units are considered to be able to deliver both active and reactive power. Moreover, it is assumed that each unit is allowed to operate within restricted power factor and non-controlled terminal voltage. The amount of available fuel is also considered, which can be adapted for modeling a diesel generator, a microturbine, or a fuel cell unit [36]. Unit commitment and power injected from DG units are represented in (23)–(28).

$$\left(P_{g,t}^{\mathrm{DG}}\right)^2 + \left(Q_{g,t}^{\mathrm{DG}}\right)^2 \le \Pi_{g,t}\left(\overline{\mathrm{S}}_g^{\mathrm{DG}}\right)^2 \quad \forall g\in\Omega_{\mathrm{DG}}, t\in\Omega_{\mathrm{T}} \tag{23}$$

$$P_{g,t}^{\mathrm{DG}} \tan\left[\cos^{-1}\left(\mathrm{pf}_g\right)\right] \ge Q_{g,t}^{\mathrm{DG}} \quad \forall g\in\Omega_{\mathrm{DG}}, t\in\Omega_{\mathrm{T}} \tag{24}$$

$$\mathrm{R}_g^{\mathrm{dw}} \le P_{g,t}^{\mathrm{DG}} - P_{g,t-1}^{\mathrm{DG}} \le \mathrm{R}_g^{\mathrm{up}} \quad \forall g\in\Omega_{\mathrm{DG}}, t\in\Omega_{\mathrm{T}}|_{t>1} \tag{25}$$

$$F_{g,t} = F_{g,t-1} - \frac{\Delta_t P_{g,t}^{\mathrm{DG}}}{\eta_g^{\mathrm{f}}\mathrm{FC}_g\mathrm{H}_g} \quad \forall g\in\Omega_{\mathrm{DG}}, t\in\Omega_{\mathrm{T}} \tag{26}$$

$$F_{g,t} \ge \underline{\mathrm{F}}_g \quad \forall g\in\Omega_{\mathrm{DG}}, t\in\Omega_{\mathrm{T}} \tag{27}$$

$$\Pi_{g,t}\in\{0,1\} \quad \forall g\in\Omega_{\mathrm{DG}}, t\in\Omega_{\mathrm{T}} \tag{28}$$

DG capacities are limited by (23), whereas (24) represent the minimum power factor limitation, guaranteeing that the injections respect the modeled capability curve. Ramp-up and ramp-down constraints are given by (25). If fuel consumption is important, the percentage of remaining fuel after each period is calculated as in (26). Equation (27) guarantees a minimum amount of fuel at end of every period. Finally, $\Pi_{g,t}$ represents the unit commitment binary variable in (28). A representation of the model used for DG units is shown in Fig. 3.

C. ESS operation

ESS are modeled as controllable sources with unitary power factor. Self-discharging rates and state of charge (SOC) are also considered by the proposed EMS. The SOC depends on the remaining energy after each period. The possible operating modes are charging (i.e., $\Phi_{b,t}=0$ and $\Lambda_{b,t}=1$); discharging (i.e., $\Phi_{b,t}=1$ and $\Lambda_{b,t}=0$), or idle ($\Phi_{b,t}=\Lambda_{b,t}=0$), given that ESS cannot charge and discharge simultaneously.

Based on the ESS operation, the SOC is calculated using (29). Minimum and maximum discharging/charging powers at period t are guaranteed by (30) and (31), respectively, both of which are controlled by the value of the binary decision variables $\Lambda_{b,t}$ and $\Phi_{b,t}$. Maximum and minimum SOC are limited by (32). A minimum SOC for specific period τ is defined as in (33). Constraint (34) guarantees that only one operating mode is allowed at each period. At last, (35) defines the binary nature of both decision variables. A representation of the model used for ESS is shown in Fig. 3.

$$\mathrm{SOC}_{b,t} = (1-\xi_b)\,\mathrm{SOC}_{b,t-1} - \frac{\Delta_t}{\mathrm{EC}_b}\left(\frac{1}{\eta_b^{\mathrm{dc}}}P_{b,t}^{\mathrm{ESS,dc}} + \eta_b^{\mathrm{ch}}P_{b,t}^{\mathrm{ESS,ch}}\right) \quad \forall b \in \Omega_{\mathrm{ESS}}, t \in \Omega_{\mathrm{T}} \quad (29)$$

$$\Phi_{b,t}\underline{P}_b^{\mathrm{dc}} \le P_{b,t}^{\mathrm{ESS,dc}} \le \Phi_{b,t}\overline{P}_b^{\mathrm{dc}} \quad \forall b \in \Omega_{\mathrm{ESS}}, t \in \Omega_{\mathrm{T}} \quad (30)$$

$$-\Lambda_{b,t}\underline{P}_b^{\mathrm{ch}} \ge P_{b,t}^{\mathrm{ESS,ch}} \ge -\Lambda_{b,t}\overline{P}_b^{\mathrm{ch}} \quad \forall b \in \Omega_{\mathrm{ESS}}, t \in \Omega_{\mathrm{T}} \quad (31)$$

$$\underline{\mathrm{SOC}}_b \le \mathrm{SOC}_{b,t} \le \overline{\mathrm{SOC}}_b \quad \forall b \in \Omega_{\mathrm{ESS}}, t \in \Omega_{\mathrm{T}} \quad (32)$$

$$\mathrm{SOC}_b^{\tau} \le \mathrm{SOC}_{b,t} \quad \forall b \in \Omega_{\mathrm{ESS}}, t \in \Omega_{\mathrm{T}}|_{t=\tau} \quad (33)$$

$$\Lambda_{b,t} + \Phi_{b,t} \le 1 \quad \forall b \in \Omega_{\mathrm{ESS}}, t \in \Omega_{\mathrm{T}} \quad (34)$$

$$\Lambda_{b,t}, \Phi_{b,t} \in \{0,1\} \quad \forall b \in \Omega_{\mathrm{ESS}}, t \in \Omega_{\mathrm{T}} \quad (35)$$

D. Proposed MISOCP model

The proposed microgrids EMS using robust convex optimization is given by (36).

$$\begin{cases} \min & (13) \\ \text{s.t.} & (14)\text{–}(35) \end{cases} \quad (36)$$

With some assumptions, the MISOCP model in (36) can be used to operate the system in both operating modes: grid-connected and isolated mode. A three-phase version of the proposed MISOCP model could be obtained by adapting the formulation in [37] to consider robust equivalents. For the sake of clarity, the proposed robust MISOCP model will be compared with a stochastic approach using the SAA [32]. The SAA model minimizes the average cost of the objective function, while binary decision variables and injections from DG units and ESS are established as first stage decision variables of the stochastic programming model.

IV. Monte Carlo Simulation and Robustness Assessment

When the microgrid is operating in grid-connected mode, the difference between local consumption and local production is assumed by the main grid and by available ESS units, guaranteeing power balance throughout the network. On the other hand, to ensure local power balance when the microgrid is in isolated mode, additional considerations are required to represent the operation of the system. In this case, the frequency and voltage droop-control of dispatchable DG units is considered, in which active and reactive power injections, along with the operation voltage from dispatchable DG units will be treated as set-points ($P_{g,t}^{\mathrm{sp}}$, $Q_{g,t}^{\mathrm{sp}}$, and $V_{g,t}^{\mathrm{sp}}$). Eventual active power fluctuations are counterweighted by the frequency-droop control, as shown in Fig. 4 to guarantee local balance, while terminal voltages follow a similar relationship for Q–V.

The participation of each unit in matching active and reactive power unbalances is usually determined by its droop configurations. The operational variations from specified set-points lead the system to a new operating frequency and voltage profile [38]–[40]. System's frequency variation is expressed in (37). While nodal voltages for DG units can be approximated using Taylor linearization around 1 pu, and calculated in (38), where $2V_{g,t} - 1 \approx V_{g,t}^{\mathrm{sqr}}$. To assure stable operation, the frequency variation must be limited by

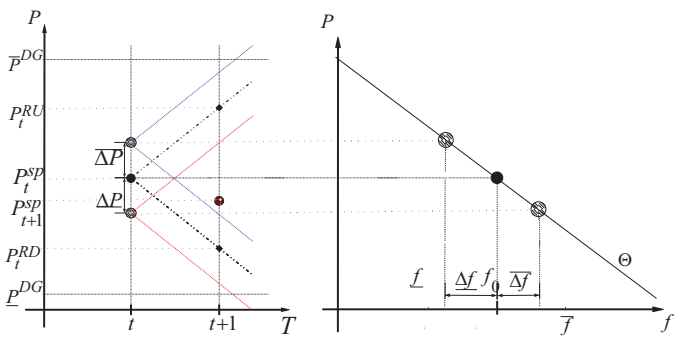

Fig. 4. Limited power variation from a specified set-point for the MCS.

(39), while voltage variations are limited indirectly by each machine's reactive availability in (24).

$$\Delta f_t = \theta_g^{\mathrm{f}}\left(P_{g,t}^{\mathrm{sp}} - P_{g,t}^{\mathrm{DG}}\right) \quad \forall g \in \Omega_{\mathrm{DG}}, t \in \Omega_{\mathrm{T}} \quad (37)$$

$$V_{g,t} = V_{g,t}^{\mathrm{sp}} - \theta_g^{\mathrm{v}}\left(Q_{g,t}^{\mathrm{DG}} - Q_{g,t}^{\mathrm{sp}}\right) \quad \forall g \in \Omega_{\mathrm{DG}}, t \in \Omega_{\mathrm{T}} \quad (38)$$

$$\underline{\Delta f} \le \Delta f_t \le \overline{\Delta f} \quad \forall t \in \Omega_{\mathrm{T}} \quad (39)$$

Once the day-ahead robust decisions have been obtained after solving (36), the binary decision variables are fixed and the active power dispatches of the DG units and the ESS are considered as desirable set-points. Thus, for each realization of the random variables generated during the MCS, the expression in (40) is minimized to simulate the real operation of the microgrid once the robust day-ahead EMS has been established. Minimizing (40) instead of (36) during the MCS guarantees that the robust decisions will only be changed if the microgrid cannot be operated with the pre-established set-points obtained by the robust convex optimization.

$$\sum_{t\in\Omega_{\mathrm{T}}}\left\{\sum_{g\in\Omega_{\mathrm{DG}}}\left(P_{g,\,t}^{\mathrm{sp}} - P_{g,\,t}^{\mathrm{DG}}\right)^2 + \sum_{b\in\Omega_{\mathrm{ESS}}}\left(P_{b,\,t}^{\mathrm{sp}} - P_{b,\,t}^{\mathrm{ESS}}\right)^2\right\} \quad (40)$$

The active power injection from dispatchable DG units is represented by $P_{g,\,t}^{\mathrm{DG}}$, and $P_{b,\,t}^{\mathrm{ESS}}$ stands for the injected or absorbed power from ESS units, both related to the MCS. Similarly, $P_{g,\,t}^{\mathrm{sp}}$ and $P_{b,\,t}^{\mathrm{sp}}$ represent the respective set-points obtained with the EMS.

The convex model used in the MCS for both operation modes is summarized in (41), where binary variables ($\Pi_{g,t}$, $\Lambda_{b,t}$, $\Phi_{b,t}$, and $\Psi_{i,t}$) are fixed to the values obtained in the robust EMS. It should be noticed that the non-convex model could be obtained by replacing the expression in (20) for $V_{j,t}^{\mathrm{sqr}} I_{ij,t}^{\mathrm{sqr}} = P_{ij,t}^2 + Q_{ij,t}^2$. However, the convergence of the optimization model is not guaranteed by non-linear solvers.

$$\begin{cases} \min & (40) \\ \text{s.t.} & (14)\text{–}(35) \text{ and } (37)\text{–}(39) \end{cases} \quad (41)$$

Finally, it is worth noting that, depending on the robust setting parameter ζ, the model in (41) might be infeasible for some realizations of the random variables generated by the MCS. In those cases, it is said that the solution was not able to prevent the microgrid from reaching an infeasible operating point. The number of feasible scenarios will be compared with the total number of simulations, from now on referred to as level of robustness.

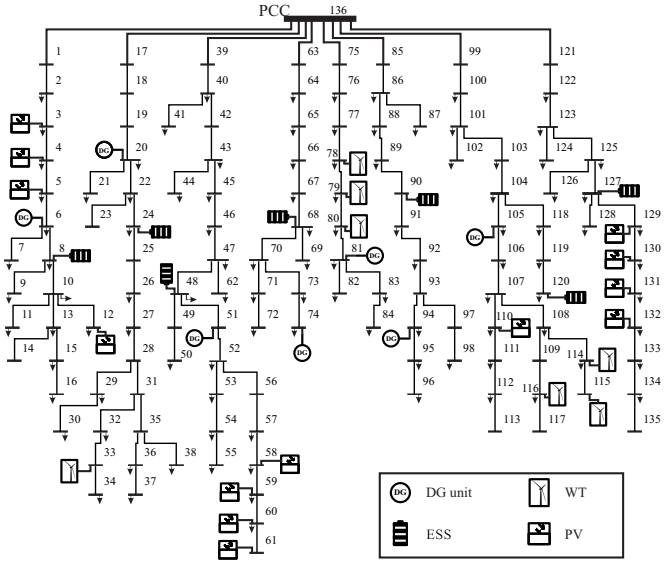

Fig. 5. 136-nodes microgrid, adapted from [41].

V. Tests and Results

A 136-node microgrid has been used to test the proposed robust EMS. It is based on a real 13.8 kV Brazilian distribution system with 136 buses, with a total peak demand of 18.31 MW and 6.95 Mvar. System parameters can be found in [41]. As shown in Fig. 5, the microgrid comprises 108 load buses, 7 dispatchable DG units, 7 ESS, 13 PV units with 600 kWp each, and 7 WT with 1.0 MW of rated power, resembling a campus area or an industrial microgrid [42]. Two tests were performed: considering grid-connected and isolated operation. Both were implemented in the mathematical programing language AMPL [43] and solved using the commercial solver CPLEX [44] using default settings on a 32 GB RAM work station with 12 threads at 2.4 GHz.

Expected values and standard deviations for solar irradiances and wind speeds were taken from [45] for the summer season. A planning horizon of 24 hours was considered, divided into one-hour periods. Loads were classified in three main groups according to their priorities: Group 1 (lowest priority) comprises nodes 1–16, 39–62, and 85–98, with $c_i^{\text{ls}} = 1.00$ \$/kWh. Group 2 (medium priority) comprises nodes 17-38, 63–74, and 99–120, with $c_i^{\text{ls}} = 3.50$ \$/kWh. Group 3 (highest priority) comprises nodes 75–84 and 121–136, with $c_i^{\text{ls}} = 7.00$ \$/kWh.

Load variation was set as 20% for both active and reactive components, and the correlation among them was set as $\rho_{i,t} = 0.50$. Data for the parameters of dispatchable DG, and ESS units, are shown in Table I.

TABLE I
Values and Units of Parameters

	Device	Parameter	Magnitude	Unit
DG units		c_g^{DG}	0.20	\$/kWh
		FC_g	1.5	m^3
		H_g	10	kWh/m^3
		η_g^{f}	35	%
		pf_g	0.9	–
		$\text{R}_g^{\text{up}} = -\text{R}_g^{\text{dw}}$	300	kW
		$\overline{\text{S}}_g^{\text{DG}}$	1.0	MVA
		θ_g^{f}	10	%
		θ_g^{v}	0.5	%
ESS units		$c_b^{\text{ESS,dc}} = c_b^{\text{ESS,ch}}$	0.60	\$/kWh
		EC_b	1.0	MWh
		ξ_b	1.0	%
		η_b^{ch}	95	%
		η_b^{dc}	97	%
		$\overline{P}_b^{\text{ch}}$	200	kW
		$\overline{P}_b^{\text{dc}}$	500	kW
		$\underline{P}_b^{\text{ch}} = \underline{P}_b^{\text{dc}}$	10	kW
		$\overline{\text{SOC}}_b$	98	%
		$\underline{\text{SOC}}_b$	10	%

A. Grid-connected mode

It was assumed that the maximum capacity of the substation is 20 MVA. The model was tested for $\zeta \in [-0.15, 0.30]$ in steps of 0.05, demanding an average execution time of 3.95 seconds to obtain each result.

For $\zeta = 0.10$, Fig. 6 shows the active load balance along the planning horizon, considering the energy injected from dispatchable DG units, PV, WT, ESS, the imported energy from the main grid, and the energy demanded from loads. Note that dispatchable DG units are only committed from periods 18–23, which are peak-load periods. Moreover, ESS only operate in charging mode before period 16 to satisfy the minimum SOC at period $\tau = 16$. It should be reminded that the charging ESS are considered as additional consumption, following the adopted convention.

As explained in Section IV, 2,000 MCS were performed to assess the robustness of each solution. Fig. 7 compares the number of feasible cases with the robustness adjustment parameter ζ. The average execution time per simulation for each MCS was 0.4 seconds.

DG units affect power flows through distribution lines. It can be seen from Fig. 8 that the total amount of energy losses increases with the level of robustness, and they are directly proportional to the objective function in every case. This is related to the commitment of more DG units to attend

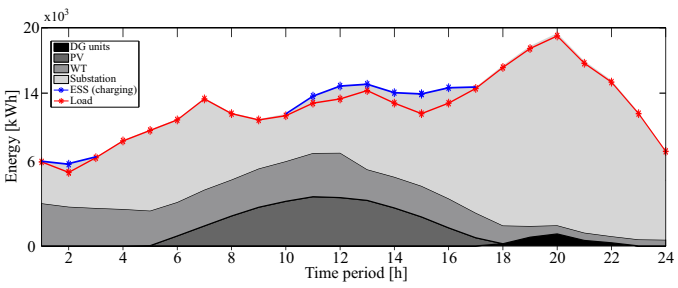

Fig. 6. Energy balance for grid-connected mode, with $\zeta = 0.10$ for an arbitrary scenario of the MCS.

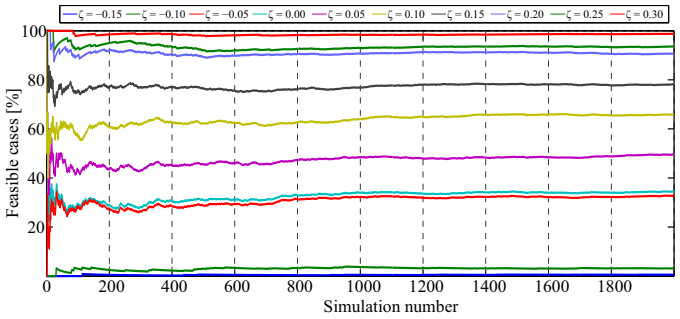

Fig. 7. Robustness assessment using Monte Carlo simulations for $\zeta \in [-0.15, 0.30]$. Grid-connected mode.

system constraints with higher robustness. When compared to the SAA model, it can be seen that the robust formulation proposed in this paper is more flexible, since the level of robustness of the solution can be modified at will, along with the resulting value of the objective function. Moreover, note that the stochastic SAA approach took more than 84 minutes to obtain a final solution, using only 100 random scenarios.

B. Isolated mode

In this case reactive power generation limits of the DG unit at bus 106 were set to $\text{pf}_{106} = 0.10$ to compensate the lack of reactive power. The model was tested for $\zeta \in [-0.15, 0.30]$ in steps of 0.05. However, there were no feasible results for the MCS when $\zeta < -0.05$, thus, only results for $\zeta \geq -0.05$ will be shown and analyzed. The average execution time for this configuration was 523 seconds to obtain each result.

As shown in the energy balance of Fig. 9, for $\zeta = 0.10$ all DG units were committed in all periods, with two peaks, one less severe at period 6 and another more pronounced at period 20. It can also be seen that ESS are operated for discharging at 1–7 and 13–20, and for charging at 9–12, coinciding with the highest energy production from PV units.

Load shedding variables involving nodes and time periods for $\zeta = 0.10$ are shown in Fig. 13, where white squares represent $\Psi_{i,t} = 0$ and blue squares $\Psi_{i,t} = 1$. Note that loads from the highest priority group (Group 3) were not disconnected at any period, while loads from the lowest priority group where curtailed in almost all of them. On the other hand, loads from Group 2 were selectively curtailed to satisfy the operational constraints in various periods.

The average percentage of energy curtailment performed by the MISOCP is shown in Fig. 10 for each time period. This is considering that 0% means that all demand was supplied, whereas 100% means that all demand was curtailed.

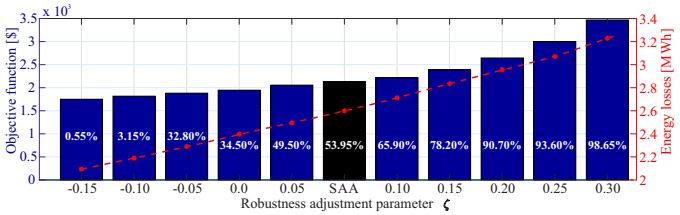

Fig. 8. Grid-connected mode: Global robustness, objective function, and energy losses for $\zeta \in [-0.15, 0.30]$ and the SAA model.

The average percentage of curtailed energy for $\zeta = 0.0$, i.e. the deterministic case, is approximately 49%, with a standard deviation of 10.5%. Similarly, the percentage of curtailed energy for $\zeta = 0.10$ is approximately $53 \pm 7.3\%$, indicating an increase in the amount of curtailed load. The mean value of the objective function is shown in Fig. 11 with the average percentage of curtailed energy and its standard deviation for different robustness setting parameters ζ. Notice that the results using the stochastic SAA approach are located between $0.05 < \zeta < 0.10$, indicating that the SAA solution is more robust and presents a higher objective function than the deterministic scenario ($\zeta = 0.0$). However, the robustness of the SAA model cannot be easily modified, and the execution time was more than 17 hours using only 100 scenarios.

It should be noticed that the objective function presented a direct relationship with the robustness level, as observed in previous tests, and as can be seen in the histograms of the objective function costs in Fig. 12, where the average execution time per simulation for each MCS was 0.69 seconds. Moreover, this results are consistent with the nature of the objective function in (13), since it is highly dependent on the quantity of curtailed energy, which also increases with the value of the robustness setting parameter.

The execution times deployed by the proposed MISOCP formulation are shown in Table II, along with the average times for one independent simulation of the MCS for both operational modes. The execution times are significantly

TABLE II
EXECUTION TIMES OF EACH TEST CASE IN SECONDS.

ζ	Grid-Connected			Isolated		
	MISOCP	MCS*	SAA	MISOCP	MCS*	SAA
−0.15	3.23	0.46		–	–	
−0.10	3.25	0.45		–	–	
−0.05	3.41	0.47		466.92	0.62	
0.0	3.56	0.43		478.69	0.63	
0.05	3.76	0.48	5,066	508.18	0.56	62,531
0.10	3.92	0.44		517.36	0.54	
0.15	4.27	0.43		534.24	0.55	
0.20	4.48	0.41		545.06	0.62	
0.25	4.70	0.44		553.76	0.66	
0.30	4.96	0.46		581.33	0.64	

* Average execution time for one independent simulation.

higher for the isolated operation mode. This is related to the characteristics of the problem, and the solver's algorithm for mixed-integer programming problems, in which negligible binary variables are pruned [44].

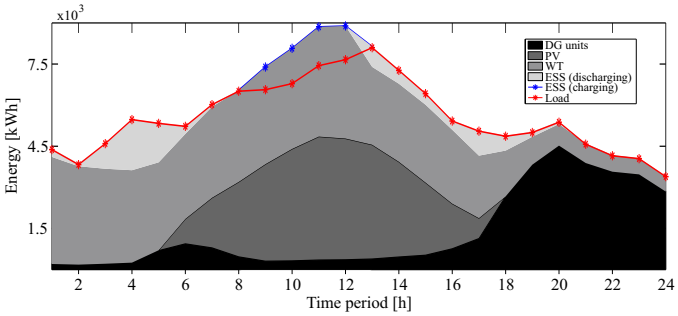

Fig. 9. Energy balance for isolated mode, with $\zeta = 0.10$ for an arbitrary scenario of the MCS.

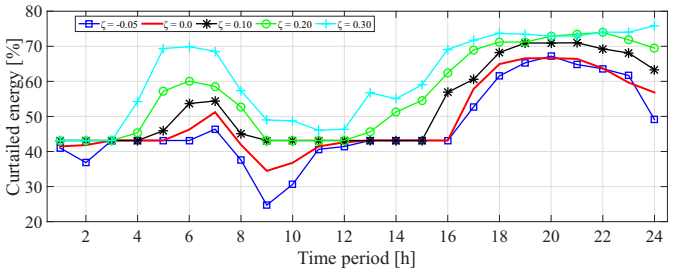

Fig. 10. Percentage of curtailed energy for different values of ζ.

VI. Conclusions

This paper presented a robust convex MISOCP model for grid-connected and isolated single-phase or balanced three-phase microgrids, considering stochasticity over the active power injections from PV units, WT units, and conventional demands. The correlation between active and reactive components of loads was contemplated. The model considers active and reactive power flows since both are essential for the operation of microgrids, voltage magnitude and current flow limits, among others. The proposed model was tested using a radial microgrids, containing 136 buses. A new simple linear robustness setting parameter was proposed to include the robust counterpart of the model by using the PDF of each stochastic variable. A procedure to find proper values for the robustness parameter was also introduced, guaranteeing that the value to be used remains between the valid interval of ζ, and providing a realistic meaning for the robustness parameter. The MCS was used to test the solutions obtained with the robust approach for 2,000 random scenarios under both operational modes. Results showed a trade-off between the robustness level obtained and the operation costs of the tested microgrid, suggesting that an optimum value of robustness depends on the risk the microgrid operator is willing to withstand. When compared to the SAA, it could be seen that the proposed formulation is more flexible and less time-consuming than the stochastic approach. Execution times were consistent with the expectations for a mixed-integer programming model, which is acceptable for offline applications since the model provides global optimal solutions. Future work can be done by considering the isolated operation of the microgrid under different contingencies, the effect of considering stochasticity in other parameters like in energy costs or in the SOC of ESS, considering unbalanced networks, among others.

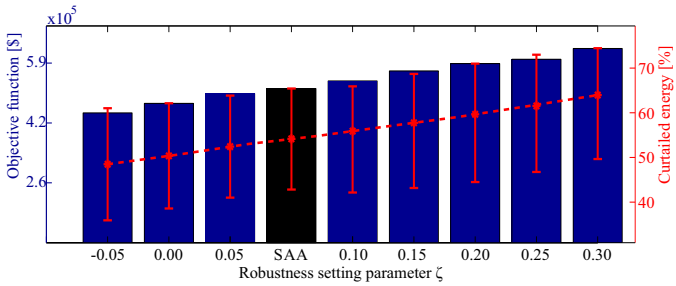

Fig. 11. Isolated mode: Objective function and load shedding for different values of ζ and the SAA model.

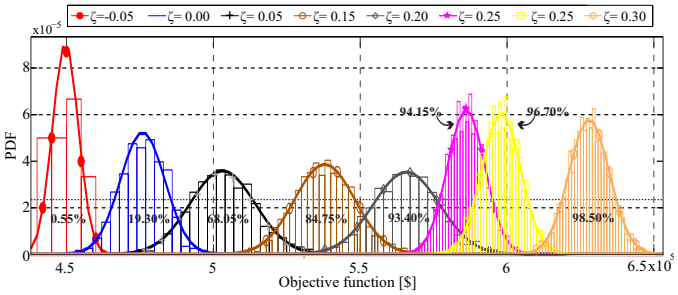

Fig. 12. Histograms of the objective function and robustness for different values of ζ. Islanded operation.

References

[1] M. Henderson, "Microgrid controllers: Their important role in the system," *IEEE Power and Energy Mag.*, vol. 15, no. 4, pp. 4–6, July 2017.

[2] R. H. Lasseter and P. Paigi, "Microgrid: a conceptual solution," in *2004 IEEE 35th Annu. Power Electron. Specialists Conf., Aachen, Germany, 20–25 Jun.* IEEE, 2004, pp. 4285–4290.

[3] Y. Xiang, J. Liu, and Y. Liu, "Robust energy management of microgrid with uncertain renewable generation and load," *IEEE Trans. Smart Grid*, vol. 7, no. 2, pp. 1034–1043, Jan. 2016.

[4] D. E. Olivares, C. A. Cañizares, and M. Kazerani, "A centralized optimal energy management system for microgrids," in *2011 IEEE Power and Energy Soc. General Meeting, San Diego, CA, USA, 24–29 Jul.*, 2011.

[5] E. Alvarez, A. C. Lopez, J. Gómez-Aleixandre, and N. de Abajo, "On-line minimization of running costs, greenhouse gas emissions and the impact of distributed generation using microgrids on the electrical system," in *2009 IEEE PES/IAS Conf. Sust. Alternative Energy, Valencia, Spain, 28–30 Sept*, 2009.

[6] A. C. Luna, N. L. Diaz, M. Graells, J. C. Vasquez, and J. M. Guerrero, "Mixed-integer-linear-programming-based energy management system for hybrid pv-wind-battery microgrids: Modeling, design, and experimental verification," *IEEE Trans. Power Electron.*, vol. 32, no. 4, pp. 2769–2783, Apr 2017.

[7] J. S. Giraldo, J. A. Castrillon, and C. A. Castro, "Energy management of isolated microgrids using mixed-integer second-order cone programming," in *2017 IEEE Power & Energy Soc. General Meeting, Chicago, IL, USA, July 16-20*. IEEE, 2017.

[8] T. Niknam, M. Zare, and J. Aghaei, "Scenario-based multiobjective volt/var control in distribution networks including renewable energy sources," *IEEE Trans. Power Del.*, vol. 27, no. 4, pp. 2004–2019, Oct. 2012.

[9] M. Bazrafshan and N. Gatsis, "Decentralized stochastic optimal power flow in radial networks with distributed generation," *IEEE Trans. Smart Grid*, vol. 8, no. 2, pp. 787–801, Mar. 2017.

[10] V. S. Tabar, M. A. Jirdehi, and R. Hemmati, "Energy management in microgrid based on the multi objective stochastic programming incorporating portable renewable energy resource as demand response option," *Energy*, vol. 118, pp. 827–839, Jan 2017.

[11] H. Farzin, M. Fotuhi-Firuzabad, and M. Moeini-Aghtaie, "A stochastic multi-objective framework for optimal scheduling of energy storage systems in microgrids," *IEEE Trans. Smart Grid*, vol. 8, no. 1, pp. 117–127, Jan. 2017.

[12] H. Shuai, J. Fang, X. Ai, Y. Tang, J. Wen, and H. He, "Stochastic optimization of economic dispatch for microgrid based on approximate dynamic programming," *IEEE Trans. Smart Grid*, to be published.

[13] A. Ben-Tal and A. Nemirovski, "Robust convex optimization," *Mathematics of operations research*, vol. 23, no. 4, pp. 769–805, Nov 1998.

[14] D. Bertsimas and M. Sim, "The price of robustness," *Operations research*, vol. 52, no. 1, pp. 35–53, Feb. 2004.

[15] J. C. López, M. Lavorato, J. F. Franco, and M. J. Rider, "Robust optimisation applied to the reconfiguration of distribution systems with reliability constraints," *IET Gener. Transm. Distrib.*, vol. 10, no. 4, pp. 917–927, Mar. 2016.

[16] Y. Zhang, N. Gatsis, and G. B. Giannakis, "Robust energy management for microgrids with high-penetration renewables," *IEEE Trans. Sust. Energy*, vol. 4, no. 4, pp. 944–953, Oct. 2013.

[17] F. Valencia, J. Collado, D. Sáez, and L. G. Marín, "Robust energy management system for a microgrid based on a fuzzy prediction interval

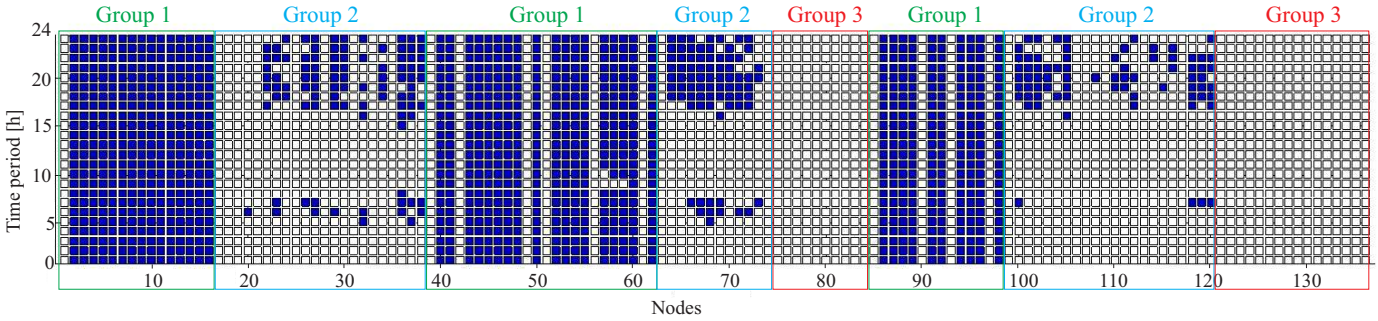

Fig. 13. Load shedding at each node for $\zeta = 0.10$. Isolated mode.

model," *IEEE Trans. Smart Grid*, vol. 7, no. 3, pp. 1486–1494, May. 2016.

[18] Y. Xu, Z. Yang, W. Gu, M. Li, and Z. Deng, "Robust real-time distributed optimal control based energy management in a smart grid," *IEEE Trans. Smart Grid*, pp. 1568–1579, July 2017.

[19] J. Liu, H. Chen, W. Zhang, B. Yurkovich, and G. Rizzoni, "Energy management problems under uncertainties for grid-connected microgrids: a chance constrained programming approach," *IEEE Trans. Smart Grid*, 2016.

[20] W. Hu, P. Wang, and H. Gooi, "Towards optimal energy management of microgrids via robust two-stage optimization," *IEEE Trans. Smart Grid*, 2016.

[21] Y. Guo and C. Zhao, "Islanding-aware robust energy management for microgrids," *IEEE Trans. Smart Grid*, vol. 9, no. 2, pp. 1301–1309, Mar. 2018.

[22] Z. Shi, H. Liang, S. Huang, and V. Dinavahi, "Distributionally robust chance-constrained energy management for islanded microgrids," *IEEE Trans. Smart Grid*, to be published.

[23] E. D. Anese, K. Baker, and T. Summers, "Chance-constrained ac optimal power flow for distribution systems with renewables," *IEEE Trans. Power Syst.*, vol. 32, no. 5, pp. 3427 – 3438, Sep. 2017.

[24] S. Pirouzi, J. Aghaei, M. A. Latify, G. R. Yousefi, and G. Mokryani, "A robust optimization approach for active and reactive power management in smart distribution networks using electric vehicles," *IEEE Syst. J.*, to be published.

[25] D. Bienstock, M. Chertkov, and S. Harnett, "Chance-constrained optimal power flow: Risk-aware network control under uncertainty," *SIAM Rev.*, vol. 56, no. 3, pp. 461–495, Aug. 2014.

[26] I. Serna-Suárez, G. Ordóñez-Plata, and G. Carrillo-Caicedo, "Microgrid's energy management syst.: A survey," in *12th Int. Conf. on the Eur. Energy Market, Lisbon, Portugal, May 19-22*, 2015.

[27] L. Gigoni *et al.*, "Day-ahead hourly forecasting of power generation from photovoltaic plants," *IEEE Trans. Sust. Energy*, vol. 9, no. 2, pp. 831–842, Apr. 2018.

[28] N. Amjady, F. Keynia, and H. Zareipour, "Short-term load forecast of microgrids by a new bilevel prediction strategy," *IEEE Trans. Smart Grid*, vol. 1, no. 3, pp. 286–294, Dec. 2010.

[29] X. Zhang and A. J. Conejo, "Robust transmission expansion planning representing long-and short-term uncertainty," *IEEE Trans. Power Syst.*, vol. 33, no. 2, pp. 1329–1338, Mar. 2018.

[30] M. Farivar and S. H. Low, "Branch flow model: Relaxations and convexification – part I," *IEEE Trans. Power Syst.*, vol. 28, no. 3, pp. 2554–2564, Aug. 2013.

[31] J. F. Franco, M. J. Rider, and R. Romero, "A mixed-integer quadratically-constrained programming model for the distribution system expansion planning," *Int. J. of Electrical Power & Energy Syst.*, vol. 62, pp. 265–272, 2014.

[32] A. J. Kleywegt, A. Shapiro, and T. Homem-de Mello, "The sample average approximation method for stochastic discrete optimization," *SIAM J. on Optimization*, vol. 12, no. 2, pp. 479–502, Dec. 2002.

[33] A. Ben-Tal and A. Nemirovski, "Robust solutions of linear programming problems contaminated with uncertain data," *Math. programming*, vol. 88, no. 3, pp. 411–424, Sept. 2000.

[34] C. Mattson and A. Messac, "Handling equality constraints in robust design optimization," in *44th AIAA/ASME/ASCE/AHS/ASC Structures, Structural Dynamics, and Materials Conf., Norfolk, VA, 7–10 Apr.*, 2003.

[35] S. Rangavajhala, A. Mullur, and A. Messac, "The challenge of equality constraints in robust design optimization: examination and new approach," *Structural and Multidisciplinary Optimization*, vol. 34, no. 5, pp. 381–401, Mar. 2007.

[36] M. Choobineh and S. Mohagheghi, "Emergency electric service restoration in the aftermath of a natural disaster," in *Proc. IEEE Glob. Humanit. Technol. Conf., Seattle, WA, USA, 8–11 Oct.* IEEE, 2015, pp. 183–190.

[37] J. Franco, L. Ochoa, and R. Romero, "Ac opf for smart distribution networks: An efficient and robust quadratic approach," *IEEE Trans. Smart Grid*, 2017.

[38] U. B. Tayab, M. A. B. Roslan, L. J. Hwai, and M. Kashif, "A review of droop control techniques for microgrid," *Renewable and Sustain. Energy Rev.s*, vol. 76, pp. 717–727, Mar. 2017.

[39] C. Li, S. K. Chaudhary, M. Savaghebi, J. C. Vasquez, and J. M. Guerrero, "Power flow analysis for low-voltage ac and dc microgrids considering droop control and virtual impedance," *IEEE Trans. Smart Grid*, vol. 8, no. 6, pp. 2754–2764, 2017.

[40] F. Mumtaz, M. Syed, M. Al Hosani, and H. Zeineldin, "A novel approach to solve power flow for islanded microgrids using modified newton raphson with droop control of dg," *IEEE Trans. Sust. Energy*, vol. 7, no. 2, pp. 493–503, Apr. 2016.

[41] J. R. Mantovani, F. Casari, and R. A. Romero, "Reconfiguração de sistemas de distribuição radiais utilizando o critério de queda de tensão," *Controle & Automação*, pp. 150–159, Sep 2000.

[42] M. Barnes *et al.*, "Real-world microgrids-an overview," in *IEEE Int. Conf. on System of Syst. Eng., San Antonio, TX, USA, 16-18 April*. IEEE, 2007.

[43] R. Fourer, D. M. Gay, and B. W. Kernighan, "A modeling language for mathematical programming," *Manage. Science*, vol. 36, no. 5, pp. 519–554, May 1990.

[44] *CPLEX optimization subroutine library guide and reference*, 1st ed. IBM ILOG Inc., Incline Village, NV, 2008.

[45] P. Kayal and C. Chanda, "Optimal mix of solar and wind distributed generations considering performance improvement of electrical distribution network," *Renewable Energy*, vol. 75, pp. 173–186, Mar. 2015.

Juan S. Giraldo received the B.Sc. degree in electrical engineering from Universidad Tecnológica de Pereira, Pereira, Colombia, in 2012, and the M.Sc. degree in electrical engineering from the University of Campinas, Campinas, Brazil, in 2015, where he is pursuing his Ph.D. degree also in electrical engineering. His current research interests include the optimization, planning, and control of modern electrical power systems.

Jhon A. Castrillon received the B.Sc. degree from the Universidad Tecnológica de Pereira, Pereira, Colombia, in 2012, and the M.Sc. degree from the University of Campinas, Campinas, Brazil, in 2015, where he is currently pursuing his Ph.D. degree, all in electrical engineering. His current research interests include the development of methodologies for the optimization, operation planning, and control of modern electrical power systems.

Juan C. López received the double B.Sc. degrees in electronical engineering and electrical engineering from the Universidad Nacional de Colombia, Manizales, Colombia, in 2011 and 2012, respectively, and the M.Sc. degree in electrical engineering from São Paulo State University, Ilha Solteira, Brazil, in 2015. He is currently pursuing the Ph.D. degree in Electrical Engineering with the University of Campinas, Campinas, Brazil. His current research interests include development of methodologies for the optimization, planning, and control of electrical distribution systems.

Marcos J. Rider (S'97–M'06–SM'16) received the B.Sc. (Hons.) and P.E. degrees from the National University of Engineering, Lima, Peru, in 1999 and 2000, respectively, the M.Sc. degree from the Federal University of Maranhão, Maranhão, Brazil, in 2002; and the Ph.D. degree from the University of Campinas (UNICAMP), Campinas, Brazil, in 2006 – all in electrical engineering. Currently, he is a Professor in the Department of Systems and Energy at UNICAMP. His areas of research are the development of methodologies for the optimization, planning, and control of electrical power systems, and applications of artificial intelligence in power systems.

Carlos A. Castro (S'90–M'94–SM'00) received the B.S. and M.S. degrees from the University of Campinas (UNICAMP), Campinas, Brazil, in 1982 and 1985, respectively, and the Ph.D. degree from Arizona State University, Tempe, in 1993. He has been with UNICAMP since 1983, where he is currently a Professor.